Gust Response Analysis for Cascades Operating in Nonuniform Mean Flows

Kenneth C. Hall* and Joseph M. Verdon†
United Technologies Research Center, East Hartford, Connecticut 06108

The unsteady aerodynamic response of a subsonic cascade subjected to entropic, vortical, and acoustic gusts is analyzed. Field equations for the first-order unsteady perturbation are obtained by linearizing the time-dependent mass, momentum, and energy conservation equations about a nonlinear, isentropic, and irrotational mean or steady flow. A splitting technique is then used to decompose the unsteady velocity into irrotational and rotational parts leading to field equations for the unsteady entropy, rotational velocity, and irrotational velocity fluctuations that are coupled only sequentially. The entropic and rotational velocity fluctuations can be described in closed form in terms of the mean-flow drift and stream functions that can be computed numerically. The irrotational unsteady velocity is described by an inhomogeneous linearized potential equation that contains a source term that depends on the rotational velocity field. This equation is solved via a finite-difference technique. Results are presented to indicate the status of the numerical solution procedure and to demonstrate the impact of blade geometry and mean blade loading on the aerodynamic response of cascades to vortical gust excitations. The analysis described herein leads to very efficient predictions of cascade unsteady aerodynamic phenomena, making it useful for turbomachinery aeroelastic and aeroacoustic design applications.

Introduction

DESTRUCTIVE forced vibrations can occur in turbomachinery blading when a periodic aerodynamic force, with frequency close to a system natural frequency, acts on the blades in a given row. A primary source of such vibrations is the aerodynamic interaction between adjacent blade rows, of which the two principal types are traditionally referred to as potential-flow interaction and wake interaction. The former results from the variations in the velocity potential or pressure field associated with the blades of a given row and their effect on the blades of a neighboring row moving at a different rotational speed. This type of interaction is of serious concern when the axial spacings between neighboring blade rows are small or flow Mach numbers are high. Wake interaction is the effect of the wakes shed by one or more upstream rows upon the flow through a given blade row. This type of interaction can be strong over large axial distances.

Until recently, the inviscid unsteady aerodynamic analyses that have been available for turbomachinery aeroelastic applications were based on classical linearized theory (for an informative review see Whitehead[1]). Here the steady and harmonic unsteady departures of the flow variables from a uniform freestream are regarded as small and of the same order of magnitude, leading to uncoupled linear constant coefficient boundary-value problems for the steady and the complex amplitudes of the unsteady disturbances. Thus, unsteady solutions based on the classical linearization are essentially restricted to cascades of unloaded flat-plate blades that operate in an entirely subsonic or an entirely supersonic environment. Very efficient semianalytic solution procedures have been developed for two-dimensional attached subsonic[2-4] and supersonic[5-8] flows and have been applied with some success in turbomachinery aeroelastic and aeroacoustic design calculations. It should also be mentioned that extensive efforts have been made to develop three-dimensional unsteady aerodynamic analyses, based on the classical linearization, for turbomachinery aeroelastic and aeroacoustic applications.[9]

Because of the limitations in physical modeling associated with the classical linearization, more general two-dimensional inviscid linearizations have been developed.[10-12] These account for the effects of important design features such as real blade geometry, mean blade loading, and operation at transonic Mach numbers on the unsteady aerodynamic response of a cascade. Here, unsteady disturbances are regarded as small-amplitude harmonic fluctuations about a nonuniform steady background flow. The steady flow is determined as a solution of a nonlinear inviscid equation set, and the unsteady flow is governed by a set of linear equations with variable coefficients that depend upon the underlying steady flow. This type of analytical model has received considerable attention in recent years, and we refer the reader to the recent articles by Verdon[13,14] for a detailed description of the theoretical formulation. Useful solution algorithms for the nonlinear steady problem are currently available, and solution methods[15] for linearized unsteady perturbations of isentropic and irrotational steady background flows have reached the stage where it is appropriate to consider them for turbomachinery aeroelastic and aeroacoustic design applications. Unfortunately, for the most part, these methods have been developed only for blade flutter and acoustic response applications. Recently, Hall and Crawley[12] used the linearized Euler equations to describe the unsteady flow in cascades subjected to wake (entropic and vortical) excitations. The linearized Euler technique, while significantly more efficient than time-marching Euler codes, is not as efficient as a linearized analysis based on the isentropic and irrotational mean flow assumptions.

If the flow is subsonic or transonic with weak shocks, then the mean flow can be regarded as irrotational and isentropic. Under these circumstances, the inviscid conservation equations can be simplified. Goldstein[16,17] expressed the linearized inviscid equations in nonconservative form and used a splitting technique to study the behavior of vortical and entropic gusts for flows in which the steady component is both irrotational and isentropic. The unsteady velocity field is split into irrotational and rotational parts leading to linear variable coefficient equations for the entropy, rotational velocity, and velocity potential. These field equations are sequentially coupled so that the entropy transport equation, the rotational

Received Feb. 19, 1990; revision received Aug. 10, 1990; accepted for publication Aug. 13, 1990.

*Research Engineer, Theoretical and Computational Fluid Dynamics. Member AIAA.

†Manager, Theoretical and Computational Fluid Dynamics. Associate Fellow AIAA.

velocity transport equation, and the elliptic velocity potential equation can be solved in order. Furthermore, closed-form solutions can be determined for the entropy and rotational velocity fluctuations. Finally, the unsteady potential is described by an inhomogeneous wave equation in which the source term depends on the rotational velocity field. The major computational expense is associated with solving the latter equation. Hence, this approach—like the linearized Euler technique—can be used to analyze the gust response problem, but it is nearly as efficient as the potential techniques used for flutter prediction. Furthermore, since the potential equation is essentially the same as that solved using the current unsteady potential codes,[10,11] the splitting technique can be incorporated into these existing codes. One drawback of Goldstein's velocity splitting technique is that the rotational velocity is singular along blade and wake surfaces for flows containing stagnation points. However, Atassi and Grzedzinski[18] have proposed a modification to Goldstein's theory that removes this singularity.

In this paper, an analysis based on Atassi and Grzedzinski's formulation is presented for subsonic cascade flows. This analysis has been implemented into an existing computer code LINFLO that can be used to predict the unsteady pressure response of realistic cascade configurations to prescribed external aerodynamic (i.e., incident entropic, vortical, and acoustic disturbances) and structural (blade motions) excitations. The analysis is applied herein to a number of cascade configurations, and the results demonstrate that mean loading has a strong effect on the unsteady aerodynamic response to incident vortical excitations.

Physical Problem

We wish to consider the aerodynamic response of a cascade, such as the one shown in Fig. 1, that interacts with incoming wakes or inlet flow distortions. The mean positions of the blade chord lines coincide with the line segments $\eta = \xi \tan\Theta + mG$, $0 \le \xi \le \cos\Theta$, $m = 0, \pm 1, \pm 2, \ldots$, where ξ and η are coordinates in the cascade axial and "circumferential" directions, respectively, m is a blade number index, Θ is the cascade stagger angle, and G is the cascade gap vector that is directed along the η axis with magnitude equal to the blade spacing. In the present discussion, all physical quantities are dimensionless. Lengths are scaled with respect to blade chord, time with respect to the ratio of blade chord to upstream freestream flow speed, density and velocity with respect to upstream freestream density and flow speed, respectively, pressure with respect to the product of the upstream freestream density and the square of the upstream freestream speed, and entropy with respect to the fluid specific heat at constant pressure.

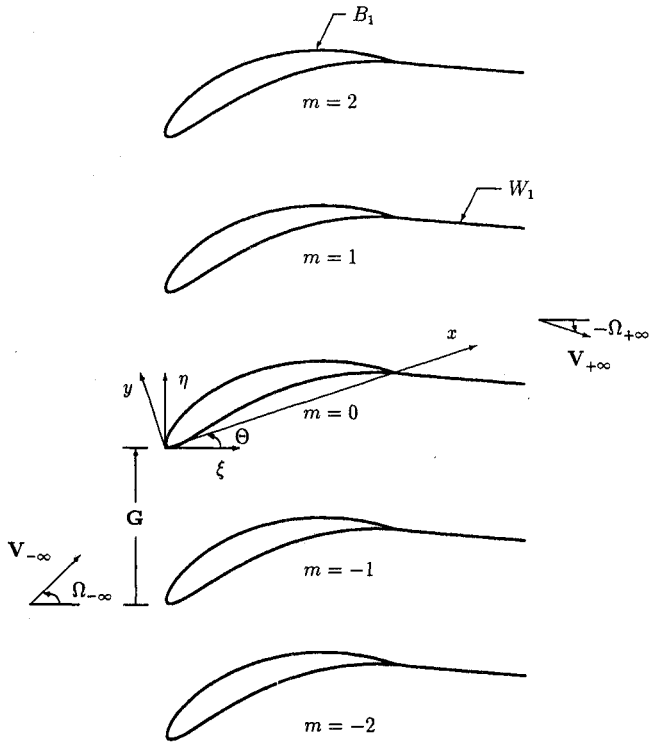

Fig. 1 Two-dimensional compressor cascade.

The time-dependent or unsteady fluctuations in the flow can arise from one or more of the following sources: blade motions, upstream and/or downstream acoustic disturbances that carry energy toward the blade row, and upstream entropic and vortical disturbances that are convected through the blade row by the mean flow. The foregoing excitations are each assumed to be of small amplitude, i.e., of order ϵ, periodic in time, and to occur at temporal frequency ω. The external aerodynamic excitations are also spatially periodic. In the present investigation, we are primarily concerned with inlet entropic and vortical disturbances. Far upstream of the blade row these disturbances are of the form

$$\tilde{s}(x,t) = Re\{s_{-\infty}\exp[i(\kappa_{-\infty}\cdot x + \omega t)]\} \quad (1)$$

$$\tilde{\zeta}(x,t) = Re\{\zeta_{-\infty}\exp[i(\kappa_{-\infty}\cdot x + \omega t)]\} \quad (2)$$

where $s_{-\infty}$ and $\zeta_{-\infty}$ are the complex amplitudes of incident entropic and vortical fluctuations, x is a position vector, and t is time. We use the symbol $\kappa_{-\infty}$ to denote the wave number of an incident disturbance. Also, the temporal frequency and wave number of an incident entropic or vortical disturbance are related by $\omega = -\kappa_{-\infty}\cdot V_{-\infty}$, where $V_{-\infty}$ is the uniform relative inlet velocity.

Unsteady Perturbations about a Potential Mean Flow

Although the actual flow through a blade row is extremely complex, i.e., viscous, heat conducting, and three-dimensional, the physics of the gust response problem in axial flow machines is dominated by inviscid effects—at least for attached flows. Hence, we assume that the fluid motion is governed by differential forms of the mass, momentum, and energy conservation laws for an inviscid perfect gas (i.e., the Euler equations). For small amplitude excitations, the time-dependent flow can be regarded as a small perturbation about an underlying nonlinear mean or steady background flow. Thus, for example, we can set

$$\tilde{V}(x,t) = V(x) + \tilde{v}(x,t) + \mathcal{O}(\epsilon^2) \quad (3)$$

Where V is the local steady velocity, and $\tilde{v}$ is the local unsteady perturbation velocity.

If we assume that the mean flow is entirely subsonic and that far upstream of the blade row it is at most a small irrotational perturbation from a subsonic uniform flow, then the background flow will be isentropic and irrotational; i.e., $V = \nabla\Phi$, where Φ is the velocity potential. The field equations that govern this underlying steady flow follow from the mass and momentum conservation laws and the isentropic relations for a perfect gas and are given by

$$\nabla\cdot(\bar{\rho}\nabla\Phi) = 0 \quad (4)$$

$$(M_{-\infty}A)^2 = \bar{\rho}^{\gamma-1} = (\gamma M^2_{-\infty}P)^{(\gamma-1)/\gamma}$$

$$= 1 - \frac{\gamma-1}{2}M^2_{-\infty}[(\nabla\Phi)^2 - 1] \quad (5)$$

where M, A, $\bar{\rho}$, and P are the local Mach number, speed of sound propagation, density, and pressure, respectively, and γ is the specific heat ratio of the fluid. Numerical procedures for determining two-dimensional steady potential flows through cascades have been developed extensively,[19,20] particularly for

flows with subsonic relative inlet and exit Mach numbers (i.e., $M_{\mp\infty}<1$).

The field equations that govern the first-order unsteady perturbation of a nonlinear isentropic and irrotational steady flow are determined from the full nonlinear time-dependent mass, momentum, and entropy-transport equations and the thermodynamic equation relating the entropy, pressure, and density of a perfect gas. After performing some straightforward algebra,[13,14] we obtain a system of differential equations for the first-order entropy ($\tilde{s}$), velocity ($\tilde{v}$), and pressure ($\tilde{p}$), respectively. These equations can be cast into a very convenient form by introducing the Goldstein velocity decomposition.[16,17] Thus, after setting $\tilde{v} = \nabla\tilde{\phi} + \tilde{v}_R$, where the unsteady potential fluctuation $\tilde{\phi}$ governs the unsteady pressure fluctuation through the relation $\tilde{p} = -\bar{\rho}\bar{D}\tilde{\phi}/Dt$, and $\bar{D}/Dt = \partial/\partial t + \nabla\Phi\cdot\nabla$ is a mean flow convective derivative operator, we find that the field equations that govern the unsteady flow variables can be written in the form

$$\frac{\bar{D}\tilde{s}}{Dt} = 0 \tag{6}$$

$$\frac{\bar{D}}{Dt}(\tilde{v}_R - \tilde{s}\nabla\Phi/2) + [(\tilde{v}_R - \tilde{s}\nabla\Phi/2)\cdot\nabla]\nabla\Phi = 0 \tag{7}$$

$$\frac{\bar{D}}{Dt}\left(A^{-2}\frac{\bar{D}\tilde{\phi}}{Dt}\right) - \bar{\rho}^{-1}\nabla\cdot(\bar{\rho}\nabla\tilde{\phi}) = \bar{\rho}^{-1}\nabla\cdot(\bar{\rho}\tilde{v}_R) \tag{8}$$

Several interesting features of these equations are worth noting. First, they are linear and contain variable coefficients that depend on the mean flow. Second, the equations for $\tilde{s}$, $\tilde{v}_R$, and $\tilde{\phi}$ are sequentially coupled. Hence, we can solve, in order, a scalar equation for the entropy, a vector equation for the rotational velocity, and a scalar equation for the velocity potential. Finally, a convection equation describes the behavior of the entropy, a modified convection equation describes the rotational velocity, and an inhomogeneous convected wave equation with a source term that depends on the rotational velocity describes the velocity potential.

This form of the governing equations is very general in that it describes the complete time-dependent first-order perturbation about an isentropic and irrotational mean flow. Most flows of interest in turbomachinery, however, are periodic in time with period T. Hence, the unsteady flow can be represented by a Fourier series in which the fundamental frequency ω is $2\pi/T$. Since the first-order equations are linear, the behavior of each Fourier component can be analyzed individually, then added together to form the total solution. Thus, without loss in generality, we could analyze the Fourier components term by term and then add the results. In this case, the time-dependent terms in Eqs. (6–8) would be replaced by the individual terms of the Fourier series, e.g., $\tilde{\phi}(x,t)\rightarrow\phi(x)\exp(i\omega t)$, and the convective derivative operator would have the form $\bar{D}/Dt = i\omega + \nabla\Phi\cdot\nabla$.

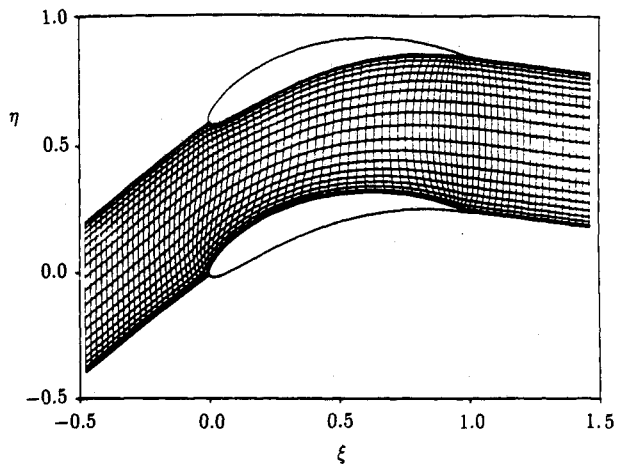

Fig. 2 Extended blade-passage solution domain and computational grid.

Using the harmonic description of the unsteady flow, the explicit time dependence can be removed from the linearized problem. Equations (6) and (7) for the entropy and rotational velocity can be solved over a single extended blade-passage region (see Fig. 2) subject to boundary conditions along the upstream far-field boundary. The potential equation, Eq. (8), requires boundary conditions around the entire domain, i.e., the upstream and downstream, far-field boundaries, the upstream periodic boundaries, and the airfoil and wake surfaces.

Entropy and Rotational Velocity Fluctuations

As demonstrated by Goldstein,[16] closed-form solutions for the entropy and rotational velocity fluctuations can be determined in terms of the drift (Δ) and stream (Ψ) functions of the steady background flow. The former measures the time required for a fluid particle to traverse the distance between points on a streamline. For the present application we define the drift and stream functions as follows:

$$\Delta(x) = \Delta(x_-) + \int_{x_- + e_N[\Psi(x)-\Psi_0]/(\bar{\rho}V)_{-\infty}}^{x} V^{-1}\,d\tau_\Psi \tag{9}$$

$$\Psi(x) = \Psi(x_-) + \int_{x_-}^{x}\bar{\rho}(e_z\times V)\cdot d\tau \tag{10}$$

In Eqs. (9) and (10) x_- is the position vector to the point of intersection (ξ_-, η_-) of the reference blade stagnation streamline and the axial line $\xi = \xi_-$, e_z is a unit vector that points out from the page, $e_N = e_z\times V_{-\infty}/V_{-\infty}$ is a unit vector normal to the upstream freestream velocity, $d\tau_\Psi$ is a differential element of arc length along a streamline, and $d\tau$ is a differential vector tangent to the path of integration in Eq. (10). The value of Δ at a given point x is determined by performing the integration in Eq. (9) along the streamline that passes through x, whereas $\Psi(x)$ is independent of the path used to evaluate the line integral in Eq. (10).

We introduce the vector

$$X - V_{-\infty}t = V_{-\infty}(\Delta - t)e_T + \Psi e_N/(\bar{\rho}V)_{-\infty} \tag{11}$$

where e_T is a unit vector pointing in the direction of the upstream freestream velocity, and the functions $\Delta - t$ and Ψ are independent material properties (or Lagrangian coordinates) of the steady background flow. Furthermore, we choose the constants $\Delta(x_-)$ and $\Psi(x_-)$ so that $X\rightarrow x$, as $\xi\rightarrow-\infty$. It follows that any arbitrary scalar or vector function, say $\mathfrak{F}$, of $(X - V_{-\infty}t)$ is convected without change by the steady background flow and that $\mathfrak{F}$ is a function of $x - V_{-\infty}t$ far upstream of the blade row, i.e.,

$$\frac{\bar{D}}{Dt}\mathfrak{F}(X - V_{-\infty}) = 0$$

$$\lim_{\xi\rightarrow-\infty}\mathfrak{F}(X - V_{-\infty}t) = \mathfrak{F}(x - V_{-\infty}t) \tag{12}$$

The foregoing considerations permit us to write immediately the solution to the entropy transport equation, Eq. (6), which satisfies the upstream condition, Eq. (1), as

$$\tilde{s}(x,t) = \tilde{s}_{-\infty}(X - V_{-\infty}t) = Re\{s_{-\infty}\exp[i\kappa_{-\infty}\cdot(X - V_{-\infty}t)]\}$$

$$= Re\{s(x)\exp(i\omega t)\} \tag{13}$$

where $s(x) = s_{-\infty}\exp(i\kappa_{-\infty}\cdot X)$ is the complex amplitude of the first-order entropy fluctuation.

The rotational velocity fluctuation can also be expressed in terms of the drift and stream functions of the steady background flow and, in this case, the prescribed upstream rota-

tional velocity distribution. For a two-dimensional irrotational background flow, the general solution to the rotational velocity transport equation, Eq. (7), is given by

$$\tilde{v}_R = \nabla \otimes X \cdot \tilde{\mathfrak{A}}(X - V_{-\infty}t) + (\tilde{s}/2)\Delta\Phi \tag{14}$$

where $\otimes$ denotes the tensor or dyadic product and $\tilde{\mathfrak{A}}$ is an arbitrary vector function. The particular solution to Eq. (7) that satisfies the far upstream condition, Eq. (2), can be obtained by setting

$$\tilde{\mathfrak{A}}(X - V_{-\infty}t) = \tilde{v}_{R,-\infty}(X - V_{-\infty}t) - \tilde{s}_{-\infty}(X - V_{-\infty}t)V_{-\infty}/2 \tag{15}$$

where $\tilde{s}_{-\infty}(X - V_{-\infty}t)$ is given in Eq. (13) and

$$\tilde{v}_{R,-\infty}(X - V_{-\infty}t) = Re\{v_{R,-\infty}\exp[i\kappa_{-\infty} \cdot (X - V_{-\infty}t)]\} \tag{16}$$

After combining Eqs. (13–16), we find that

$$\tilde{v}_R(x,t) = Re\{[\nabla \otimes X \cdot \mathfrak{A}_{-\infty} + s_{-\infty}\nabla\Phi/2] \times \exp[i\kappa_{-\infty} \cdot (X - V_{-\infty}t)]\} = Re\{v_R(x)\exp(i\omega t)\} \tag{17}$$

where $\mathfrak{A}_{-\infty} = v_{R,-\infty} - s_{-\infty}V_{-\infty}/2$ and $v_R(x)$ is the complex amplitude of the rotational velocity fluctuation.

Modification to the Goldstein Splitting

At this point we have expressed the entropy and rotational velocity fluctuations in terms of the mean flow drift and stream functions. Therefore, these fluctuations and the source term $\bar{\rho}^{-1}\nabla \cdot (\bar{\rho}\tilde{v}_R)$ in the unsteady potential equation can be evaluated once the drift and stream functions, and their derivatives, are determined from a solution for the underlying steady flow. However, as pointed out by Goldstein and later by Atassi and Grzedzinski,[18] if the background flow has leading-edge stagnation points, the rotational velocity will be singular along blade and wake surfaces. Such behavior is a result of the singular behavior of the drift function, i.e., $\Delta \to a_0 \ell n\, n$ as $n \to 0$, where n is the normal distance from the airfoil or wake surface, and a_0 is a constant that describes the behavior of the flow in the vicinity of the stagnation point.

Consider the perturbation velocity

$$\tilde{v} = \nabla\tilde{\phi} + \tilde{v}_R \tag{18}$$

Atassi and Grzedzinski showed that if one used the velocity decomposition

$$\tilde{v} = (\nabla\tilde{\phi} - \nabla\tilde{\phi}^*) + (\tilde{v}_R + \nabla\tilde{\phi}^*) = \nabla\tilde{\phi}' + \tilde{v}_R' \tag{19}$$

where $\tilde{\phi}^*$ is a pressureless or convected potential, i.e., $D\tilde{\phi}^*/Dt = 0$, then $\tilde{v}_R'$ satisfies the same transport equation, Eq. (7), as $\tilde{v}_R$. Similarly, $\tilde{\phi}'$ satisfies the same field equation, Eq. (8), as $\tilde{\phi}$. Furthermore, if one chooses $\tilde{\phi}^*$ carefully, $\tilde{v}_R'$ will be regular on the blade and wake surfaces. In particular, if we set

$$\tilde{\phi}^* = Re\{[-i\omega^{-1}\mathfrak{A}_{-\infty} \cdot V_{-\infty} + F(Y)]\exp[i\kappa_{-\infty} \cdot (X - V_{-\infty}t)]\} \tag{20}$$

the rotational velocity $\tilde{v}_R$ is given by

$$\tilde{v}_R' = Re\left\{\left[\nabla \otimes X \cdot i\kappa_{-\infty}F + \left(c_2 + \frac{dF}{dY}\right)\nabla Y + s_{-\infty}\nabla\Phi/2\right]\exp[i\kappa_{-\infty} \cdot (X - V_{-\infty}t)]\right\} \tag{21}$$

Here $c_2 = -\omega^{-1}V_{-\infty}(\kappa_{-\infty} \times \mathfrak{A}_{-\infty}) \cdot e_z$, $Y = \Psi/(\bar{\rho}V)_{-\infty}$, and $F(Y)$ is a function that depends on, among other things, the behavior of the mean flow in the vicinity of a stagnation point. In particular, we set

$$F(Y) = \frac{(\kappa_{-\infty} \times \mathfrak{A}_{-\infty}) \cdot e_z G\cos\Omega_{-\infty}}{2\pi(\omega/V_{-\infty})(1 - ia_0\omega)} \sin\left[\frac{2\pi(Y - Y_0)}{G\cos\Omega_{-\infty}}\right] \tag{22}$$

This choice of F eliminates the singular behavior from the rotational velocity v_R' and ensures that $v_R' \cdot n \equiv 0$ at blade and wake surfaces; however, the source term $\bar{\rho}^{-1}\nabla \cdot (\bar{\rho}\tilde{v}_R')$ is still singular at such surfaces.

Equations (13) and (21) relate the first-order unsteady entropy $\tilde{s}$ and rotational velocity v_R' to the prescribed inlet quantities $s_{-\infty}$, $v_{R,-\infty}$, and $\kappa_{-\infty}$ and to the velocity, drift function, and stream function of the steady background flow. Note that $\tilde{v}_R'$ depends on Δ and Ψ and the first partial derivative of these functions. Therefore, the unsteady vorticity $\nabla \times \tilde{v}_R'$ and the source term $\bar{\rho}^{-1}(\nabla \cdot \bar{\rho}\tilde{v}_R')$ depend also on the second partial derivatives of the mean-flow drift and stream functions. Thus, an accurate solution for the nonlinear steady background flow is a critical prerequisite to properly determining the unsteady effects associated with inlet entropic and vortical excitations.

Numerical Solution Procedure

The theoretical foundation for the present linearized analysis has been outlined. We will proceed to discuss the procedures used to determine the complex amplitudes of the unsteady entropy s, rotational velocity v_R', and source term $\bar{\rho}^{-1}\nabla \cdot (\bar{\rho}\tilde{v}_R')$. The finite-difference numerical model used to solve the boundary-value problem for the complex amplitude of the unsteady potential ϕ' has been described in previous work. Since the only changes required for the gust problem are those needed to accommodate the source term in the field equation, Eq. (8), and rotational velocity effects in the far-field boundary conditions, we will not repeat the description here, but simply refer the reader to Refs. 11, 21, and 22 for the details.

Generation of Streamline Grid

The unsteady entropy and rotational velocity have been expressed in terms of the drift and stream functions Δ and Ψ of the underlying steady flow. For this reason it is convenient, but not essential, to use an H grid in which one set of mesh lines are the streamlines of the steady background flow for the numerical evaluation of these unsteady flow variables. The first step in the grid generation process is to specify the grid point locations on the boundary of the physical solution domain, i.e., the single extended blade-passage region of finite extent shown in Fig. 2. The boundaries of this region are the suction and pressure surfaces of the blades, the upstream and downstream stagnation streamlines, and the upstream and downstream axial lines $\xi = \xi_{\mp}$.

Once the boundary points for the H grid have been determined, the locations of the interior points are found using an elliptic grid generation technique similar to that developed by Thompson et al.[23] An elliptic grid generator offers the advantages that relatively smooth grids can be determined and grids for complicated flow geometries, such as those associated with cascades of thick, highly cambered blades, are easy to generate. Following Thompson et al., the grid lines are described by the partial differential equations

$$\nabla^2\Xi = \mathcal{P}, \qquad \nabla^2\mathfrak{K} = \mathcal{Q} \tag{23}$$

The "axial" and "streamwise" grid lines correspond to lines of constant Ξ and $\mathfrak{K}$, respectively. The functions $\mathcal{P}$ and $\mathcal{Q}$ can be used to control the spacing and orthogonality of the grid lines. In this investigation, however, we have chosen the function $\mathcal{Q}$ so that $\mathfrak{K}$ is the stream function Ψ of the irrotational steady background flow, i.e., $\mathcal{Q}e_z = V \times \nabla\bar{\rho}$.

Rather than solve Eqs. (23) for Ξ and Ψ as functions of ξ and η, we invert these equations to determine ξ and η as functions of Ξ and Ψ. The resulting nonlinear partial differen-

tial equations for ξ and η are solved numerically, using a successive line over-relaxation procedure, over a rectangular region in Ξ, Ψ space, subject to Dirichlet conditions on ξ and η at the boundary. The values of ξ and η along the boundary of the rectangular domain are defined by their values at the prescribed points along the boundary of the extended blade-passage domain. In the present investigation, nonconstant transformed grid spacings are used to control the spacings in the physical plane. For example, by choosing appropriate values of $\Delta\Xi_i$ and $\Delta\Psi_j$, the streamwise and axial grid lines can be packed near blade and wake surfaces and near the leading and trailing edges of the blades, respectively.

A typical grid generated for a compressor cascade operating at an inlet Mach number of 0.3 and an inlet flow angle of 40.0 deg is shown in Fig. 2. The blades are thick and highly cambered, and the cascade has a gap-to-chord ratio G of 0.6 and a stagger angle Θ of 15 deg. The steady flow, which is determined using the analysis of Caspar,[19] is used to generate the stagnation streamlines and to determine the function $\mathcal{Q}$ in Eq. (23). For the grid shown, the function $\mathcal{P}$ has been set equal to 0. Note the clustering of streamlines near the blade and wake surfaces and axial lines in the vicinity of the blade leading and trailing edges, which is achieved by employing nonconstant rectangular grid spacings, $\Delta\Xi_i$ and $\Delta\Psi_j$, in the transformed plane.

Drift Function

Because a streamline mesh is used, the drift function can be evaluated by straightforward numerical integration of Eq. (9). The procedure is simply to specify the drift function along the far upstream boundary $\xi = \xi_-$ and then to evaluate this function along each streamline using the second-order difference approximation

$$\Delta_{i+1,j} = \Delta_{i,j} + \frac{\tau_{i+1,j} - \tau_{i,j}}{0.5\,(V_{i+1,j} + V_{i,j})} \tag{24}$$

Since the steady flow speed V appears in the denominator of the integrand in Eq. (9), the drift function will be singular at flow stagnation points. Hence, for a blade having a blunt leading edge, this function will be singular along the entire surface of each blade and its wake.

The calculated drift and stream function contours for the compressor cascade of Fig. 2 are shown in Fig. 3. Note that the drift function contours are orthogonal to the streamlines far upstream of the blade row. This is not a requirement, but it does simplify certain parts of the formulation. Note also the singular behavior indicated by the drift function contours near the blade and wake surfaces.

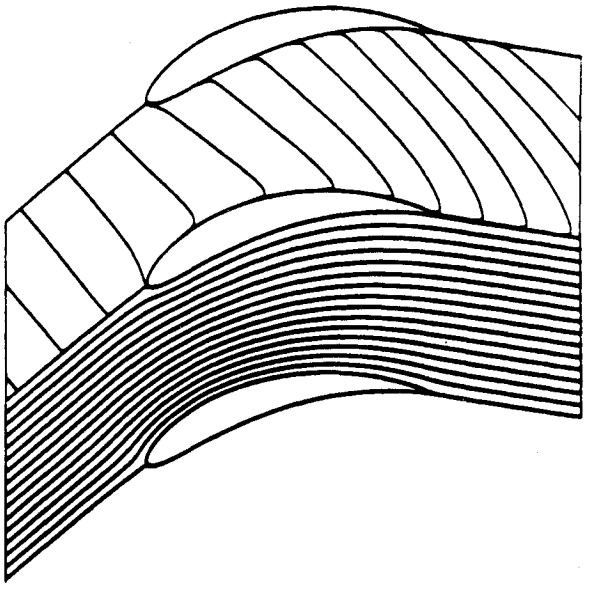

Fig. 3 Drift and stream contours for steady two-dimensional cascade flow.

The derivatives of the drift and stream functions at a given grid point are determined using the finite-difference operators developed by Caspar and Verdon.[21] Because the drift function is singular along blade and wake surfaces, one-sided difference approximations are used to evaluate its derivatives at the nodes on the first streamlines away from these surfaces. The derivatives of the drift function at blade and wake surfaces are singular but are not required to evaluate v_R' and $\bar{\rho}^{-1}\nabla\cdot(\bar{\rho}v_R')$ on these surfaces or in the field.

As noted previously, a numerical resolution of the linear, variable-coefficient, unsteady, boundary-value problem that governs the velocity potential is required over a single extended blade-passage region of finite extent. The field equation, Eq. (8), must be solved in continuous regions of the flow subject to boundary or jump conditions that are imposed at the mean positions of the blade and wake surfaces. Also, the unsteady near-field numerical solution must be matched to far-field analytical solutions[24] at finite axial distances ($\xi = \xi_\mp$) upstream and downstream from the blade row. The numerical procedures for determining ϕ' are described in Refs. 11, 21, and 22.

Numerical Results

Unsteady aerodynamic response predictions are given next to demonstrate important features of the foregoing linearized analysis. We will consider flat-plate cascades and cascades consisting of blades that are constructed by superposing the thickness distribution of a NACA four-digit series airfoil on a circular arc camber line. For the latter, H_T is the blade thickness and H_C is the height of the circular-arc camber line at blade midchord. The flows to be considered here are entirely subsonic. The steady background flows have been determined using the methods of Caspar.[19] In each case, a Kutta condition has been applied at blade trailing edges, and therefore only inlet uniform flow information, e.g., $M_{-\infty}$ and $\Omega_{-\infty}$, must be specified for the steady calculation. With one exception, the first-harmonic unsteady solutions were determined on an H-type mesh (see Fig. 2) consisting of 120 "axial" lines and 30 mean-flow streamlines. Denser meshes are usually required for resolving unsteady flows at high subsonic inlet Mach number and high frequency. In the present study, a 180×50 mesh was used to calculate an unsteady flow at $M_{-\infty} = 0.7$ and $\omega = 5$ through a flat-plate cascade. In each case, the grid lines were "packed" near the blade and wake surfaces and near the blade edges, respectively.

We first consider flat-plate cascades in which the blade mean positions are aligned with the inlet freestream flow direction, i.e., $\Theta = \Omega_{-\infty}$, to compare present response predictions with those based on Smith's[4] classical linearized analysis. We will then consider cascades of uncambered NACA airfoils to study the effects of blade thickness on the unsteady aerodynamic response to an incident vortical gust. Finally, we will examine the response of a more realistic cascade configuration: a compressor exit guide vane (EGV) consisting of thick, highly cambered blades ($H_T = 0.12$, $H_C = 0.13$).

We are primarily interested in linearized unsteady flows excited by vortical gusts, such as those that arise, for example, from wakes off the blades of an adjacent upstream blade row. If the "circumferential" spacing between the blades in the adjacent upstream row is G_{EXC} and if these blades move at velocity $V_{EXC}\boldsymbol{e}_\eta$ relative to the blade row under consideration, then the interblade phase angle (i.e., the difference in the phase of a disturbance from one blade to the next) and temporal frequency of the fundamental or blade passing vortical excitation are $\sigma = \kappa_{\eta,-\infty}G = -2\pi G/G_{EXC}$ and $\omega = -\kappa_{\eta,-\infty}V_{EXC} = \sigma G^{-1}V_{EXC}$, where $\kappa_{\eta,-\infty} = -2\pi/G_{EXC}$ is the circumferential wave number of the excitation. For the present study, we will choose $\sigma = -2\pi$, $\omega = 5$, and $\nu_g = (1,0)$ to describe a "standard"

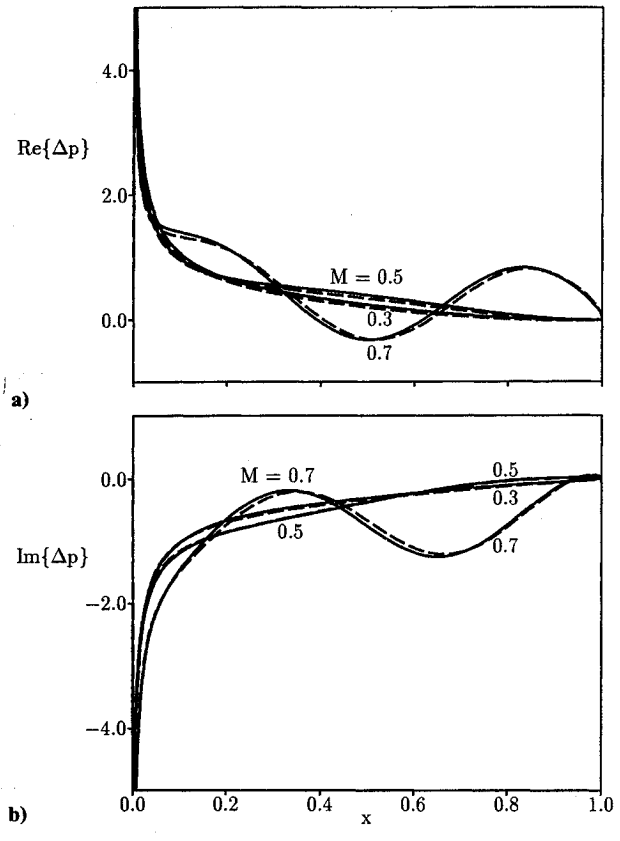

Fig. 4 Effect of Mach number on the unsteady pressure-difference response of a flat-plate cascade with $\Omega = \Theta = 45$ deg and $G = 1$ subjected to an incident vortical gust with $v_g = (1,0)$, $\omega = 5$, and $\sigma = -2\pi$: a) in-phase component (real part) of Δp; b) out-of-phase component (imaginary part); - - - Smith[4] analysis, —— present analysis.

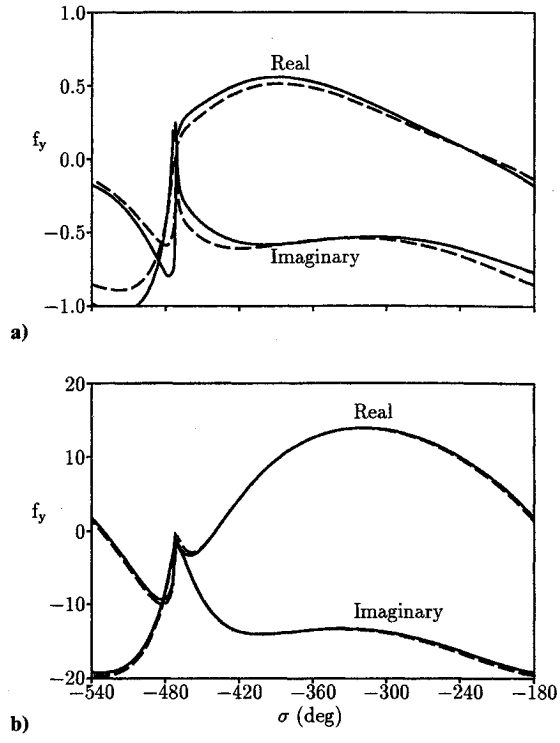

Fig. 5 Unsteady lift vs interblade phase angle for a flat-plate cascade with $M = 0.3$, $\Omega = \Theta = 45$ deg, and $G = 1$: a) unsteady lift due to incident vortical gusts with $v_g = (1,0)$ and $\omega = 5$; b) unsteady lift due to blade bending vibrations with $h_y = (1,0)$ and $\omega = 5$; - - - Smith[4] analysis, —— present analysis.

vortical gust. Here, v_g is the complex amplitude of the gust velocity component normal to the inlet freestream flow direction at the point $(x,y) = (0,0)$. Note that v_g is the amplitude at the leading edge of the reference blade that would exist if the incident gust was convected through the blade row, without distortion, by the uniform inlet flow.

A significant advantage of the present analysis is that unsteady aerodynamic response information for realistic cascades can be determined efficiently and economically. For example, a complete unsteady flow calculation on a 120×30 mesh requires about 70 s of CPU time on an APOLLO 10000 work station. Of this time, 60 s are required to construct the H grid, interpolate steady background flow information onto this grid, and set up the 25 and 9 point difference stencils used to evaluate the source term $\bar{\rho}^{-1}\nabla\cdot(\bar{\rho}v_R')$ and the unsteady potential ϕ', respectively. This information can be saved and re-used in subsequent unsteady flow calculations at different frequencies and interblade phase angles. The latter require only about 10 s of CPU time for each unsteady case.

Flat-Plate Cascade

The example flat-plate cascade has a stagger angle Θ of 45 deg, a blade spacing G of 1.0, and operates at three different inlet Mach numbers, i.e., $M_{-\infty} = 0.3$, 0.5, and 0.7. In each case the inlet flow angle $\Omega_{-\infty}$ is 45 deg and vortical excitations with $v_g = (1,0)$ and $\omega = 5$ are imposed far upstream of the blade row. Note that since the inlet freestream flow is aligned with the blade mean positions, the local steady Mach number, $M(=M_{-\infty})$, and flow angle, $\Omega(=\Omega_{-\infty})$, are constants for the flat-plate configuration. Predicted unsteady pressure-difference distributions $\Delta p(x)$ acting on the reference ($m = 0$) blade for the standard vortical excitation at $\sigma = -2\pi$ are shown in Fig. 4, where the solid and dashed curves represent the results of the present and of Smith's analysis, respectively. Recall that in the present analysis the unsteady potential equation contains the source term $\bar{\rho}^{-1}\nabla\cdot(\bar{\rho}v_R')$ and $\nabla\phi'\cdot\boldsymbol{n} = 0$ on blade and wake surfaces, whereas in the classical linearization the potential equation is homogeneous, and the normal component of the irrotational velocity must cancel the normal component of the gust velocity at blade surfaces. The results in Fig. 4 show that the two analyses yield pressure-difference predictions that are in very good agreement. The 120×30 mesh was used to calculate the unsteady flows at $M_{-\infty} = 0.3$ and $M_{-\infty} = 0.5$, but because of the high wave number acoustic response associated with the unsteady flow at $M_{-\infty} = 0.7$ and $\omega = 5$, a denser, i.e., 180×50, mesh was required to predict the unsteady flow at $M_{-\infty} = 0.7$.

The unsteady lift f_y responses at the reference blade of the flat-plate cascade operating at $M_{-\infty} = 0.5$ to prescribed vortical excitations with $v_g = (1,0)$ and $\omega = 5$ and to prescribed blade translations, $h_y \exp(i\omega t)$, normal to the blade chord with $h_y = (1,0)$ and $\omega = 5$ are plotted vs interblade phase angle in Fig. 5. The excitations occur over interblade phase range extending from -540 deg (-3π) to -180 deg $(-\pi)$. Abrupt changes in the lift response curves occur at $\sigma = -473.8$ deg (-2.62π) and -471.1 deg (-2.63π). The excitations at these interblade phase angles produce resonant acoustic response disturbances in the far field. The lift responses to the vortical excitations predicted by the numerical and semianalytic solution procedures are in good agreement; however, this agreement is not nearly as good as that between the lift responses to the blade translational motions, suggesting that the present numerical analysis still requires some improvements so that the source term $\bar{\rho}^{-1}\nabla\cdot(\bar{\rho}v_R')$ can be evaluated more accurately.

Effects of Blade Thickness

We proceed to evaluate the present analysis by applying it to a family of cascade configurations. Here $\Theta = 45$ deg, $G = 1$, the blades are uncambered ($H_C = 0$), but the blade thickness varies from $H_T = 0$ to 0.12. These cascades operate at an inlet Mach number of 0.3 and an inlet flow angle of 45 deg and are

subjected to the standard vortical excitation at $v_g = (1,0)$, $\omega = 5$, and $\sigma = -2\pi$.

This cascade family has been studied to examine the effects of blade thickness on the unsteady aerodynamic response to a vortical gust. It should be noted that although the blades are uncambered and their chord lines are aligned with the inlet flow direction, i.e., $\Theta = \Omega_{-\infty}$, there is a small mean or steady lift force acting on the blades for $H_T \neq 0$. This force increases in magnitude, from 0 for $H_T = 0$ to 0.062 for $H_T = 0.12$, with increasing blade thickness. The exit Mach numbers ($M_{+\infty}$) vary from 0.3 for $H_T = 0$ to 0.314 for $H_T = 0.12$; the exit flow angles ($\Omega_{+\infty}$) from 45 to 47.22 deg. The unsteady pressure-difference distributions along the reference blades of the cascades with $H_T = 0$, 0.04, 0.08, and 0.12 are shown in Fig. 6. These results indicate that blade thickness has only a limited impact on the aerodynamic response to a vortical excitation, at least for the low-speed flows considered here. Indeed, the pressure-difference response for the cascade of 2% thick blades (not shown) closely resembles that for the flat-plate ($H_T = 0$) cascade. This result provides an important check on the present analysis, indicating that the mathematical difficulties associated with mean flow stagnation at blade leading edges have been successfully overcome.

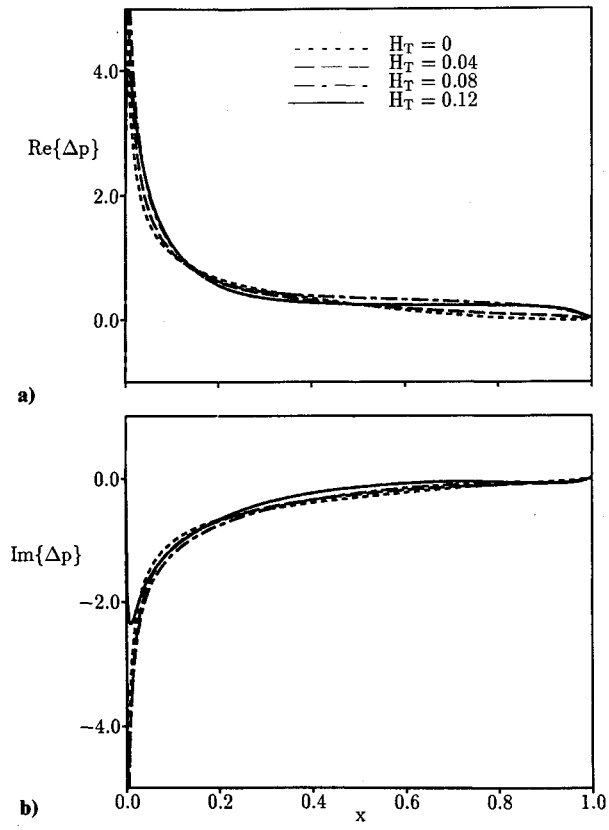

Fig. 6 Effect of blade thickness on the unsteady pressure-difference response of NACA 00XX cascades with $M_{-\infty} = 0.3$, $\Omega_{-\infty} = 45$ deg, $\Theta = 45$ deg, and $G = 1$ subjected to an incident vortical gust with $v_g = (1,0)$, $\omega = 5$, and $\sigma = -2\pi$: a) and b) as in Fig. 4.

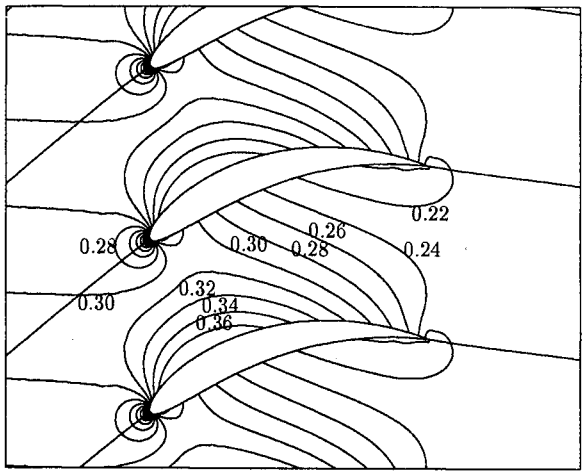

Fig. 7 Mach number contours for steady flow with $M_{-\infty} = 0.3$ and $\Omega_{-\infty} = 40$ deg through the EGV cascade ($\Theta = 15$ deg, $G = 0.6$, $H_T = 0.12$, and $H_C = 0.13$).

Exit Guide Vane

We turn now to a more realistic configuration, i.e., we consider the compressor EGV that consists of thick, $H_T = 0.12$, highly cambered, $H_C = 0.13$, NACA four digit airfoils. The EGV has a stagger angle of 15 deg and a blade spacing of 0.6 and operates at a prescribed inlet Mach number and inlet flow angle of 0.3 and 40 deg, respectively. The calculated exit Mach number, exit flow angle, and mean lift force F_y acting on each blade are 0.226, −7.4 deg, and 0.36, respectively. Steady Mach number contours for this configuration are depicted in Fig. 7.

We will examine the unsteady pressure response of this cascade to incident vortical excitations and compare it to that for a corresponding flat-plate cascade with $\Theta = \Omega_{-\infty} = 40$ deg, $G = 0.6$, and $M_{-\infty} = 0.3$. Contours of the real part of the

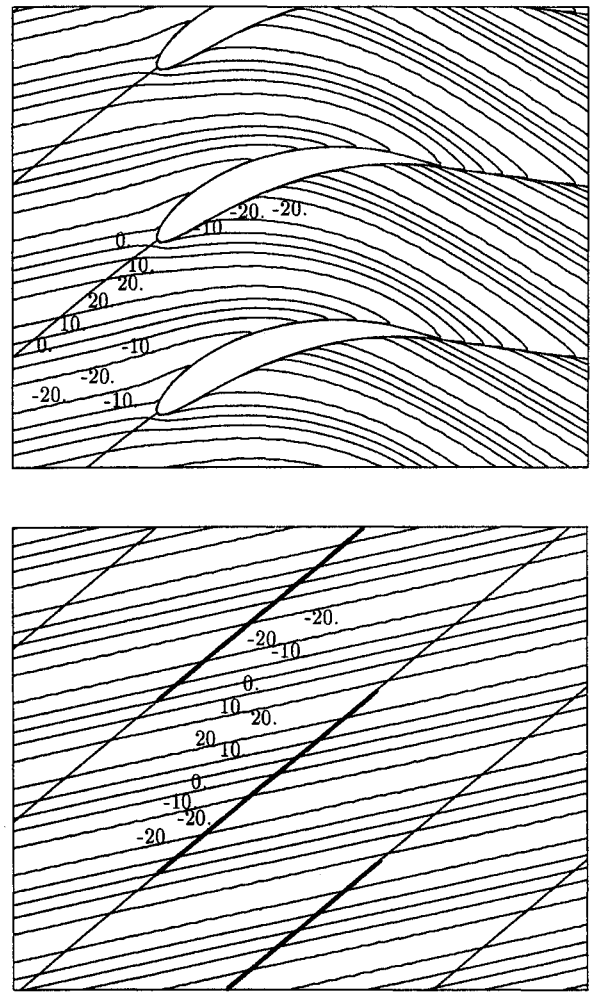

Fig. 8 Contours of the real part of the unsteady vorticity for the EGV and the corresponding flat-plate ($M = 0.3$, $\Omega = \Theta = 40$ deg, $G = 0.6$) cascades subjected to an incident vortical gust with $v_g = (1,0)$, $\omega = 5$, and $\sigma = -2\pi$.

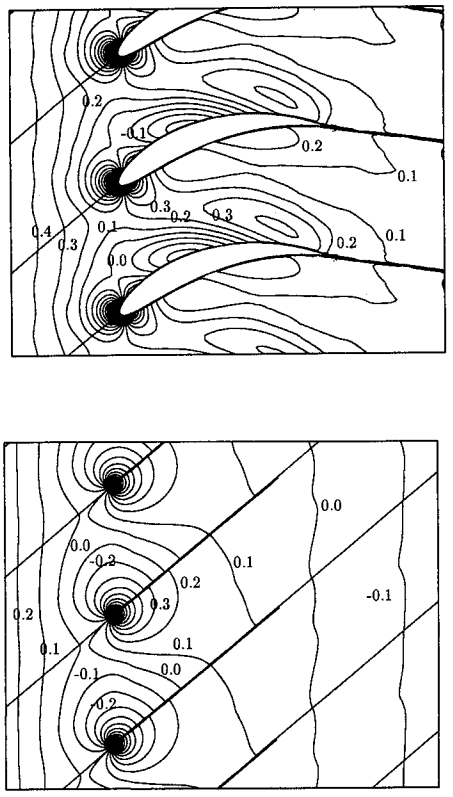

Fig. 9 Contours of the in-phase unsteady pressure for the EGV and the corresponding flat-plate cascades subjected to an incident vortical gust with $v_g = (1,0)$, $\omega = 5$, and $\sigma = -2\pi$.

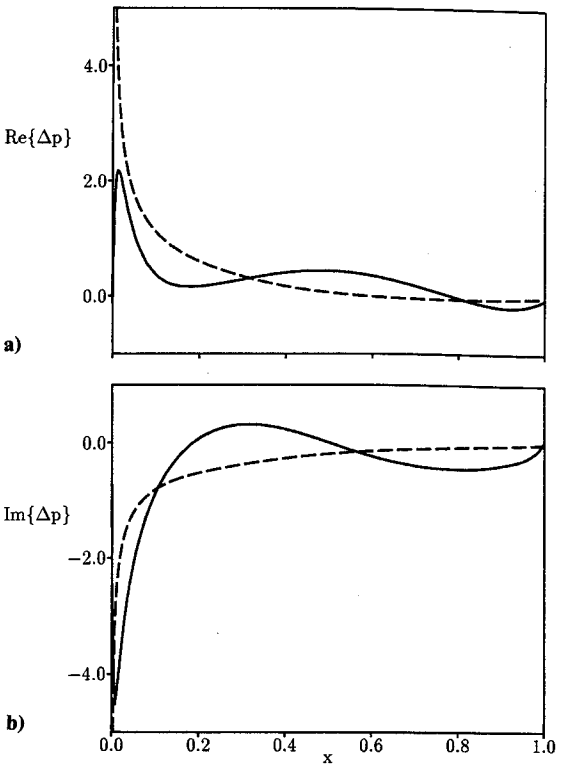

Fig. 10 Unsteady pressure-difference response for the EGV and the corresponding flat-plate cascades subjected to an incident vortical gust with $v_g = (1,0)$, $\omega = 5$, and $\sigma = -2\pi$: a) in-phase component; b) out-of-phase component; - - - flat-plate cascade, —— EGV cascade.

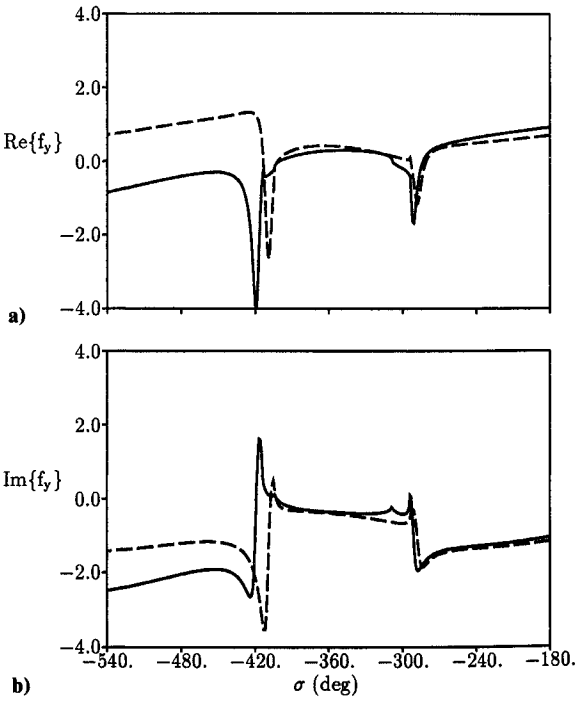

Fig. 11 Unsteady lift vs interblade phase angle for the EGV and corresponding flat-plate cascades subjected to incident vortical gusts with $v_g = (1,0)$ and $\omega = 5$: a), b), - - - , and —— as in Fig. 10.

complex amplitude of the unsteady vorticity and pressure for unsteady flows through the EGV and the corresponding flat-plate cascade are shown in Figs. 8 and 9, respectively. Here, the unsteady flows are excited by the standard vortical gust. The prescribed gust is severely distorted as it is convected by the nonuniform mean flow through the EGV blade row. In contrast, this same gust is convected without distortion by the uniform mean flow through the flat-plate cascade. The contours depicted in Fig. 9 indicate that the unsteady pressure behaviors associated with the EGV and flat-plate cascades are similar far upstream but differ substantially in the vicinity of the blade surfaces and downstream of the blade row.

The pressure-difference responses along the reference blades of the EGV and flat-plate cascades to the standard vortical excitation at $v_g = (1,0)$, $\omega = 5$, and $\sigma = -2\pi$ are shown in Fig. 10. The unsteady lift forces acting on the reference blades of the two cascades are plotted vs interblade phase angle for vortical excitations at $v_g = (1,0)$, $\omega = 5$, and $-540 \text{ deg} \leq \sigma \leq -180$ deg in Fig. 11. The excitations at $\sigma = -404.2$ and -293.9 deg produce resonant acoustic response disturbances far upstream and far downstream of the flat-plate cascade and far upstream of the EGV; those at $\sigma = -414.3$ and -308.8 deg produce such response disturbances far downstream of the EGV. The results in Figs. 10 and 11 indicate, to some extent, the relative importance of nonuniform mean flow phenomena on the local and global unsteady aerodynamic response at a blade surface for cascades subjected to incident vortical excitations. It should be noted that the unsteady lift acts in the direction of the positive y axis (see Fig. 1), and this is inclined at different angles relative to the axial flow direction for the EGV ($\Theta = 15$ deg) and flat-plate ($\Theta = 40$ deg) cascades. Also, the flat plate pressure-difference distributions in Fig. 10 are in very good agreement with the corresponding results of Smith's analysis. The flat-plate lift distributions in Fig. 11 are in good agreement with Smith's results, except for interblade phase angles lying in the range $-540 \text{ deg} < \sigma < -404.2$ deg, where the out-of-phase lift responses, i.e., $Im(f_y)$, predicted by the two analyses are similar qualitatively but show small quantitative differences.

One important effect clearly shown in Fig. 11 is that steady loading causes the unsteady lift response to be nonperiodic in interblade phase angle, i.e., $f_y(\sigma \pm 2\pi n) \neq f_y(\sigma)$. In classical theory, the aerodynamic response of the cascade depends only on the upwash induced by the gust at the blade surfaces. Since

this upwash is periodic in σ, so is the response. For loaded airfoils, the response depends on the induced upwash and on the distortion of the gust within the blade passages. This distortion is nonperiodic in σ, resulting in a nonperiodic lift response.

Concluding Remarks

A method for predicting the linearized unsteady aerodynamic response of a cascade of airfoils subjected to external aerodynamic excitations has been presented. The unsteady flow is regarded as a small perturbation of a nonuniform isentropic and irrotational steady background flow. Goldstein's splitting[16,17] along with a recent modification introduced by Atassi and Grzedzinski[18] are used to decompose the linearized unsteady velocity into irrotational and rotational parts leading to equations for the linearized unsteady entropy, rotational velocity, and velocity potential that are coupled only sequentially. The entropic and rotational velocity fluctuations are described in terms of the mean-flow drift and stream functions, and the potential fluctuation is governed by an inhomogeneous convected wave equation in which the source term depends on the rotational velocity field. In this paper the analytical and numerical techniques used to determine the linearized unsteady flow have been outlined and demonstrated through a series of numerical examples.

The results obtained using the present analysis were found to be in very good agreement with the results of Smith's classical linearized analysis for flat-plate cascades. Results for the cascades of symmetric NACA 00XX airfoils show reasonable trends with varying blade thickness and indicate that, at least for low speed flows, blade thickness has only a limited impact on the response of a cascade to incident vortical gusts. More importantly, the blade thickness study also indicates that the present analysis overcomes the mathematical difficulties associated with unsteady vortical perturbations of potential mean flows containing leading-edge stagnation points.

More detailed gust response predictions have been presented for a compressor exit guide vane, including contours of vorticity and pressure that illustrate the manner in which a vortical gust is distorted as it is convected, by the mean flow, through a blade row and the unsteady pressure response that is excited by the interaction of this gust with the blade row. These numerical results serve to demonstrate the capabilities of the present analysis for predicting the unsteady pressure response of cascades operating under high mean load conditions. This analysis leads to very efficient predictions of the aerodynamic response of realistic cascade configurations to unsteady aerodynamic excitations. Therefore, it should be useful in turbomachinery aeroelastic and aeroacoustic design studies.

Acknowledgments

This work was supported by NASA Lewis Research Center under Contract NAS3-25425 with George Stefko serving as NASA Program Manager. The authors are indebted to H. M. Atassi of the University of Notre Dame and J. Scott of the NASA Lewis Research Center for offering important insights on the velocity decomposition techniques used herein. They would also like to thank R. Rudewicz for her help in running the LINFLO code and in preparing this paper. The original version of this paper was presented at an AGARD Specialists Meeting on Unsteady Aerodynamic Phenomena in Turbomachines, held in Luxembourg, August 1989, and published in AGARD CP 468, February 1990.

References

[1]Whitehead, D. S., "Classical Two-Dimensional Methods," *AGARD Manual on Aeroelasticity in Axial-Flow Turbomachines, Unsteady Turbomachinery Aerodynamics*, Vol. 1, edited by M. F. Platzer and F. O. Carta, AGARD-AG-298, March 1987, Chap. III.

[2]Whitehead, D. S., "Vibration and Sound Generation in a Cascade of Flat Plates in Subsonic Flow," Engineering Dept., Cambridge Univ., Cambridge, England, UK, Rept. CUED/A-Turbo/TR 15, 1970.

[3]Kaji, S., and Okazaki, T., "Propagation of Sound Waves Through a Blade Row, II. Analysis Based on the Acceleration Potential Method," *Journal of Sound and Vibration*, Vol. 11, No. 3, 1970, pp. 355–375.

[4]Smith, S. N., "Discrete Frequency Sound Generation in Axial Flow Turbomachines," British Aeronautical Research Council, London, R&M 3709, 1971.

[5]Verdon, J. M., "Further Developments in the Aerodynamic Analysis of Unsteady Supersonic Cascades, I. The Unsteady Pressure Field, II. Aerodynamic Response Predictions," *Transactions of the ASME, A: Journal of Engineering for Power*, Vol. 99, No. 4, 1977, pp. 509–525.

[6]Nagashima, T., and Whitehead, D. S., "Linearized Supersonic Unsteady Flow in Cascades," British Aeronautical Research Council, London, R&M 3811, 1978.

[7]Adamczyk, J. J., and Goldstein, M. E., "Unsteady Flow in a Supersonic Cascade with Subsonic Leading Edge Locus," *AIAA Journal*, Vol. 16, No. 12, 1978, pp. 1248–1254.

[8]Ni, R. H., "A Rational Analysis of Periodic Flow Perturbation in Supersonic Two-Dimensional Cascade," *Transactions of the ASME, A: Journal of Engineering for Power*, Vol. 101, No. 3, 1979, pp. 431–439.

[9]Namba, M., "Three-Dimensional Flows," *AGARD Manual on Aeroelasticity in Axial-Flow Turbomachines, Unsteady Turbomachinery Aerodynamics*, Vol. 1, edited by M. F. Platzer and F. O. Carta, AGARD-AG-298, March 1987, Chap. IV.

[10]Whitehead, D. S., "The Calculation of Steady and Unsteady Transonic Flow in Cascades," Engineering Dept., Cambridge Univ., Cambridge, England, UK, Rept. CUED/A-Turbo/TR 118, 1982.

[11]Verdon, J. M., and Caspar, J. R., "A Linearized Unsteady Aerodynamic Analysis for Transonic Cascades," *Journal of Fluid Mechanics*, Vol. 149, Dec. 1984, pp. 403–429.

[12]Hall, K. C., and Crawley, E. F., "Calculation of Unsteady Flows in Turbomachinery Using the Linearized Euler Equations," *AIAA Journal*, Vol. 27, No. 6, 1989, pp. 777–787.

[13]Verdon, J. M., "Linearized Unsteady Aerodynamic Theory," *AGARD Manual on Aeroelasticity in Axial Flow Turbomachines, Unsteady Turbomachinery Aerodynamics*, Vol. 1, edited by M. F. Platzer and F. O. Carta, AGARD-AG-298, March 1987, Chap. II.

[14]Verdon, J. M., "Unsteady Aerodynamics for Turbomachinery Aeroelastic Applications," *Unsteady Transonic Aerodynamics*, edited by D. Nixon, Vol. 120, Progress in Astronautics and Aeronautics, AIAA, Washington, DC, 1989, pp. 287–347.

[15]Acton, E., and Newton, S. G., "Numerical Methods for Unsteady Transonic Flow," *AGARD Manual on Aeroelasticity in Axial-Flow Turbomachines, Unsteady Turbomachinery Aerodynamics*, Vol. 1, edited by M. F. Platzer and F. O. Carta, AGARD-AG-298, March 1987, Chap. VI.

[16]Goldstein, M. E., "Unsteady Vortical and Entropic Distortions of Potential Flows Round Arbitrary Obstacles," *Journal of Fluid Mechanics*, Vol. 93, Part 3, Dec. 1978, pp. 433–468.

[17]Goldstein, M. E., "Turbulence Generated by the Interaction of Entropy Fluctuations with Non-Uniform Mean Flows," *Journal of Fluid Mechanics*, Vol. 93, Part 2, July 1979, pp. 209–224.

[18]Atassi, H. M., and Grzedzinski, J., "Unsteady Disturbances of Streaming Motions Around Bodies," *Journal of Fluid Mechanics*, Vol. 209, Dec. 1989, pp. 385–403.

[19]Caspar, J. R., "Unconditionally Stable Calculation of Transonic Potential Flow Through Cascades Using an Adaptive Mesh for Shock Capture," *Transactions of the ASME, A: Journal of Engineering for Power*, Vol. 105, No. 3, 1983, pp. 504–513.

[20]Whitehead, D. S., and Newton, S. G., "A Finite Element Method for the Solution of Two-Dimensional Transonic Flows in Cascades," *International Journal for Numerical Methods in Fluids*, Vol. 5, Feb. 1985, pp. 115–132.

[21]Caspar, J. R., and Verdon, J. M., "Numerical Treatment of Unsteady Subsonic Flow Past an Oscillating Cascade," *AIAA Journal*, Vol. 19, No. 12, 1981, pp. 1531–1539.

[22]Usab, W. J., Jr., and Verdon, J. M., "Advances in the Numerical Analysis of Linearized Unsteady Cascade Flows," American Society of Mechanical Engineers, New York, ASME Paper 90-GT-11, June 1990.

[23]Thompson, J. F., Thames, F. C., and Mastin, W., "A Code for Numerical Generation of Boundary-Fitted Curvilinear Coordinate Systems on Fields Containing Any Number of Arbitrary Two-Dimensional Bodies," *Journal of Computational Physics*, Vol. 24, No. 3, 1977, pp. 274–302.

[24]Verdon, J. M., "The Unsteady Flow in the Far Field of an Isolated Blade Row," *Journal of Fluids and Structures*, Vol. 3, No. 2, 1989, pp. 123–149.